# Electronic Supplementary Information

# Interface Engineering in Cu-CoO Heterostructure for High-Efficiency Electrocatalytic Nitrate Reduction to Ammonia

Zhengguo Qu,[a,b] Shengbo Zhang,*[b,c] Zhixian Mao,[b,c] Min Liu,[b,c] Li Zhou,[b,c] Haimin Zhang,[b,c] Fengquan Song,[a] Zhongjun Li,[a] Qiong Tang,*[a] Tongfei Shi*[b,c]

[a] School of Physics, Hefei University of Technology, Hefei 230009, China

[b] Institute of Solid State Physics, HFIPS, Chinese Academy of Sciences, Hefei 230031, China

[c] University of Science and Technology of China, Hefei 230026, China

* Corresponding author: E-mail: tfshi@issp.ac.cn; jennytq@hfut.edu.cn; shbzhang@issp.ac.cn

## 1. Experimental Section

### 1.1. Chemicals and materials

Carbon nanotube bundled multi-walled were purchased from Shanghai Macklin Biochemical Co., Ltd. $Co(NO_3)_2·6H_2O$, $CuSO_4·5H_2O$ were purchased from Sinopharm Chemical Reagent Co., Ltd. $KNO_3$ (99.0%), sodium nitroferricyanide(III) dehydrate ($C_5FeN_6Na_2O·2H_2O$, 99.0%), sodium citrate ($C_6H_5Na_3O_7·2H_2O$, 99.0%), KOH (96.0%), ethylene glycol ($(CH_2OH)_2$, 99.0%), glycolic acid ($C_2H_4O_3$, 99.0%), salicylic acid ($C_7H_6O_3$, 99.5%), NaClO (available chlorine ≥ 5.0%), $NH_4Cl$ (99.5%), thiosemicarbazide ($CH_5N_3S$, 99.0%), p-aminobenzenesuifonamide ($NH_2C_6H_4SO_2NH_2$, 95.0%), N-(1-naphthyl) ethylenediamine dihydrochloride ($C_{10}H_7NHC_2H_4NH_2·2HCl$, 95.0%), $^{15}KNO_3$ (AR), $^{14}NH_4Cl$ (AR), $^{15}NH_4Cl$ (AR), were purchased from Shanghai Aladdin Biochemical Technology Co., Ltd. Shanghai. All solutions were prepared using deionized water (Millipore Corp., 18.2 MΩ cm). Commercial carbon paper (CP, HCP030N) was purchased from Shanghai Hesen Electric Co. Ltd.

### 1.2. Synthesis of Cu-CoO@CNT, Cu@CNT and Co@CNT

The synthesis procedure for Cu-CoO@CNT is illustrated in Fig. 1. Initially, 10 mM $Co(NO_3)_2·6H_2O$ and 20 mM $Cu(NO_3)_2·5H_2O$ were dissolved in 100 mL of deionized water and stirred for 2 hours. Subsequently, 1 g of carbon nanotubes (CNT) was added to the solution and the mixture was stirred for an additional 30 minutes, followed by sedimentation. After decanting the supernatant, the precipitate was collected and dried in an oven at 60°C for 12 hours. The dried material was then ground into a fine powder and transferred to a tubular furnace. The powder was calcined under

the $N_2$ atmosphere at a heating rate of 2°C/min. At 600°C, the temperature was maintained for 2 hours, after which the sample was annealed to room temperature, removed, and ground again. The final product yielded Cu-CoO@CNT.

The preparation methods for Cu@CNT and Co@CNT were similar to that of Cu-CoO@CNT, with the only difference being that the precursor solution contained solely $Cu^{2+}$ or $Co^{2+}$, respectively, for the synthesis of Cu@CNT and Co@CNT.

**1.3. Material characterization**

The scanning electron microscopy (SEM) images were obtained using SU8020 (Hitachi, Japan). The transmission electron microscopy (TEM) images were obtained using JEMARM 200F. The aberration-corrected high-angle annular dark-field scanning transmission electron microscopy (HAADF-STEM) measurements andenergy-dispersive X-ray (EDX) spectroscopy were performed using JEMARM200F. X-ray diffraction (XRD) patterns were acquired using Philips X'pert PRO with Cu Ka radiation (λ = 1.5418 Å) at 40 kV and 40 mA. Nitrogen adsorptiondesorption isotherms were measured using Autosorb-iQ-Cx. X-ray photoelectron spectroscopy (XPS) analysis was performed on an ESCALAB 250 X-ray photoelectron spectrometer (Thermo, America). Electrochemical measurements All the electrochemical measurements were performed on a CHI 660E electrochemical workstation (CH Instrumental Corporation, Shanghai, China) using an H-type cell, which was separated by a Nafion 211 proton exchange membrane. The Nafion 211 membrane was treated at 80 °C in $H_2O_2$ (5 wt.%) and 0.5 M $H_2SO_4$ aqueous solution in turn to protonate and then rinsed with deionized water before use. The catalyst inks were prepared by dispersing

5 mg sample into 500 μL of ethanol, 450 μL of water and 50 μL of Nafion (5 wt.%) under ultrasonic for 30 min, and then were loaded on a carbon paper (1.0×1.0 $cm^2$) as the working electrode with 0.25 mg $cm^{-2}$ catalyst. The saturated Ag/AgCl electrode was used as the reference electrode and a platinum mesh was used as the counter electrode. Before use, the working electrode was activated in 0.1 M KOH + 0.25 M $KNO_3$ solution. Unless otherwise stated, all experiments were performed in 0.1 M KOH + 0.25 M $KNO_3$ solution. All measured potentials versus Ag/AgCl were transformed into the potentials versus reversible hydrogen electrode (RHE) according to the following equation:

$$E_{RHE} = E_{Ag/AgCl} + 0.059\,pH + E^{0}{}_{Ag/AgCl}$$

where the $E_{Ag/AgCl}$ is the equilibrium potential under standard conditions and $E^0_{Ag/AgCl}$ = 0.197 V versus RHE at 25℃.

**1.4. Determination of ammonia.**

The concentration of the produced ammonia was detected by the indophenol blue method.[1] In detail, taken 100 μL of electrolyte in a cathode cell after 2 h electrocatalysis, and then added 9900 μL of deionized water in a 15 ml colorimetric tube. Subsequently, 500 μL of coloring agent (composed of 10 g salicylic acid, 10g sodium citrate, 55 ml 2.0 M sodium hydroxide with deionized water in 200 ml solution), 100 μL of oxidizing solution (containing 5ml sodium hypochlorite and 45ml 2.0 M sodium hydroxide in 50 ml solution), and 100 μL of catalyst solution (1.0 g $Na_2[Fe(CN)_5NO]\cdot 2H_2O$ diluted to 100 mL with deionized water) were added to the measured sample solution in turn. After the color development for 1h at room temperature, the absorbance measurements were performed by UV-Vis spectrophotometer at a wavelength of 697.5 nm. The

obtained calibration curve was used to calculate the ammonia concentration.

**1.5. Determination of nitrite.**

The produced nitrite in the electrolyte was detected by the Griess method.[2] In detail, the N-(1-naphthyl) ethylenediamine dihydrochloride (1 g), sulfonamide (20 g) and $H_3PO_4$ (50 mL, 85%) were dissolved in 250 ml of deionized water and then set the mixture to 500 ml volumetric flask to form the Griess reagent. Added 1 ml of reacted electrolyte with 9 ml of deionized water into a 15 ml colorimetric tube then mixed with 200 μL of Griess reagent and placed for 20 min at room temperature. UV-vis spectrophotometer was used to measure the absorbance of the generated nitrite at the wavelength of 540 nm. Then the concentration of $NO_2^-$ was obtained by the calibration curve.

**1.6. Calculation of NtrRR Performance**

$R_{NH_3}$, $FE$ and $S_{NH_3}$ are calculated by the following formulas:

$$Yield\ Rate_{NH3}(\mu g\ h^{-1}\ mg_{cat.}^{-1}) = \frac{C_{NH3}(\mu g\ mL^{-1}) \times V(mL)}{t(h) \times m_{cat.}(mg)}$$

$$FE\ (\%) = \frac{8 \times n_{NH_3}(mol) \times F(C\ mol^{-1})}{Q\ (C)} \times 100\%$$

$$S_{NH_3}(\%) = \frac{\Delta C_{N\text{-}NH_3}}{\Delta C_{N\text{-}NH_3} + \Delta C_{N\text{-}NO_2^-}} \times 100\%$$

$C_{NH_3}$ is the concentration of produced $NH_3$ and V is the volume of electrolyte. t is the electrolysis time, $S$ is the area of the loaded electrocatalyst, $F$ is the faradaic constant (96485 C $mol^{-1}$) and $Q$ is the total charge transferred during electrolysis. $C_{N-NH_3}$ is the concentration of produced $N-NH_3$ and $N-NO_2^-$ is the concentration of produced -$NO_2^-$.

$R_{NO_2^-}$ and $FE$ are calculated by the following equations:

$$Yield\ Rate_{NO_2^-}(\mu g\ h^{-1}\ mg_{cat.}) = \frac{C_{NO_2^-}(\mu g\ mL^{-1}) \times V(mL)}{t(h) \times m_{cat.}(mg)}$$

$$FE\ (\%) = \frac{2 \times n_{NO_2^-}(mol) \times F(C\ mol^{-1})}{Q\ (C)} \times 100\%$$

where, $C_{NO_2^-}$ and V are the measured $NO_2^-$ concentration and the electrolyte solution volume, respectively, t is the electrolysis period and $m_{cat.}$ is the amount of the loaded electrocatalyst, $F$ is the faradaic constant (96485 C $mol^{-1}$) and $Q$ is the total charge transferred during electrolysis period.

### 1.7. $^{15}N$ Isotope Labelling Experiments

For quality assurance required, $^{15}N$ isotopic labelling experiments were conducted using 0.1 M KOH + 0.25 M $K^{15}NO_3$ as the electrolyte with identical experimental procedure as that of Ar-saturated 0.1 M KOH + 0.25 M $K^{14}NO_3$ experiments. For $^1H$ NMR method, $D_2O$ (99.9 atom% D, Aladdin Biochemical Technology Co., Ltd. Shanghai) used as internal standard. The yielded $^{15}NH_3$ were analyzed by the $^1H$ NMR methods using Bruker Avance-400 MHZ.

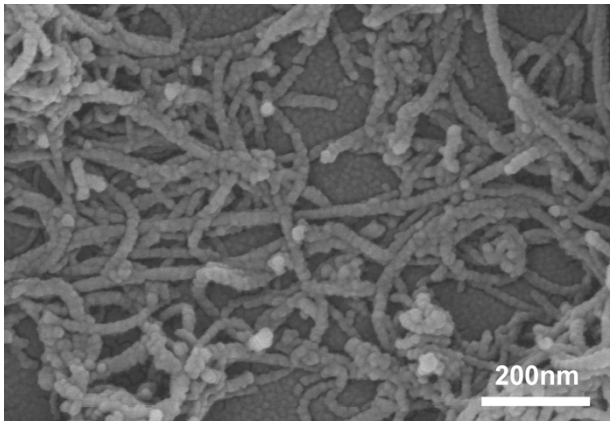


**Fig. S1** SEM image of Cu-CoO@CNT.

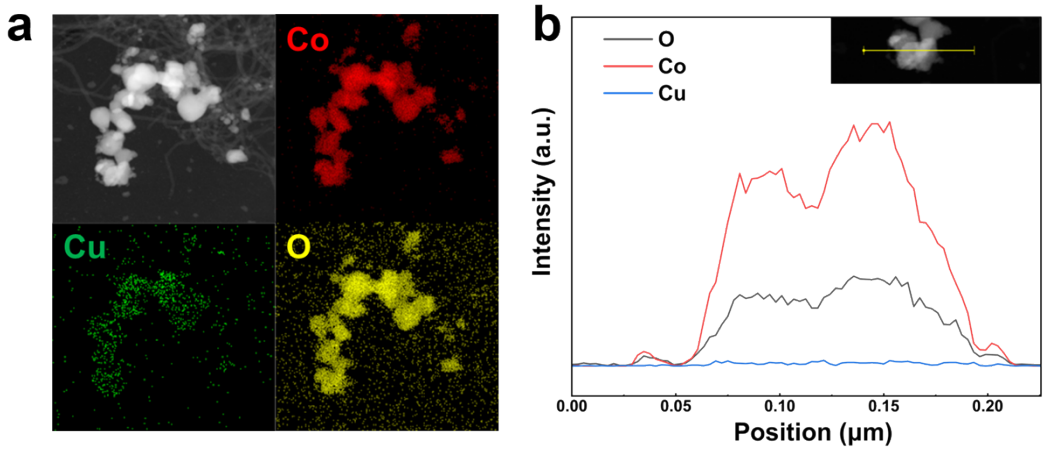


**Fig. S2** (a) EDS images of Cu-CoO@CNT. (b) EDS elemental line-scanning profile of Cu, Co and O.

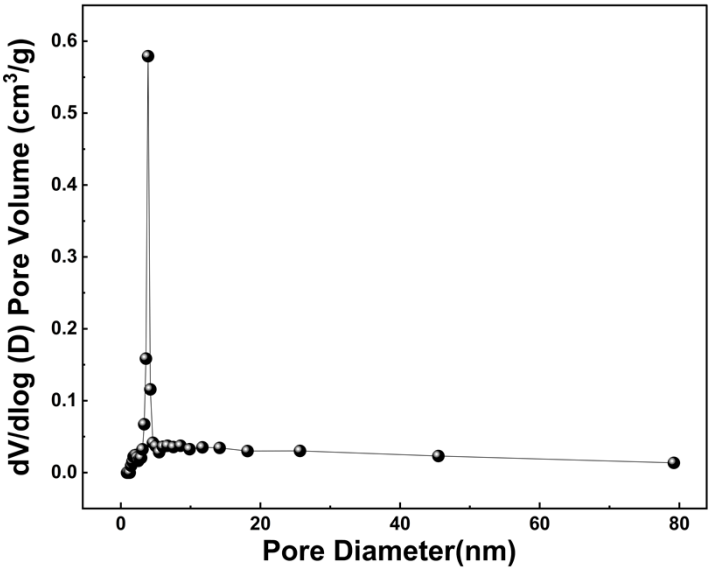


**Fig. S3** corresponding pore size distribution curve of Cu-CoO@CNT.

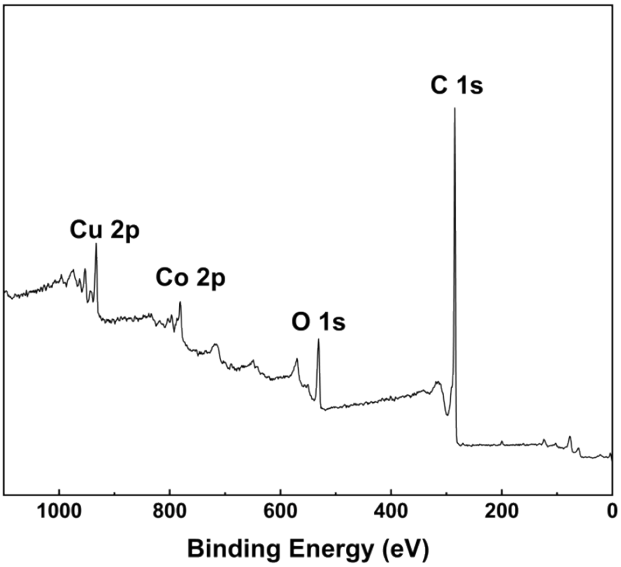


**Fig. S4** Surface survey XPS spectra of the Cu-CoO@CNT sample.

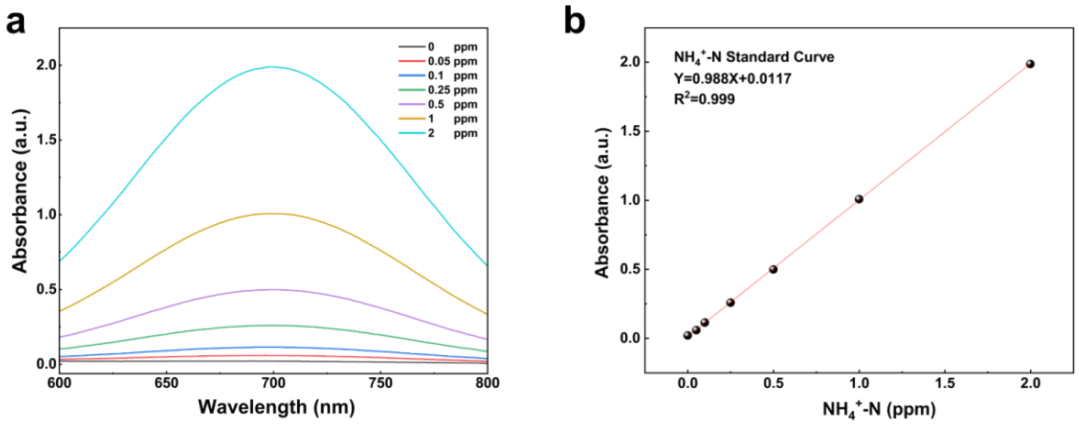


**Fig. S5** (a) UV-Vis absorption spectra obtained from the solutions with different $NH_4^+$-N concentrations (0, 0.05, 0.1, 0.25, 0.5, 1.0 and 2.0 ppm). (b) Calibration curve used to determine $NH_4^+$-N concentration.

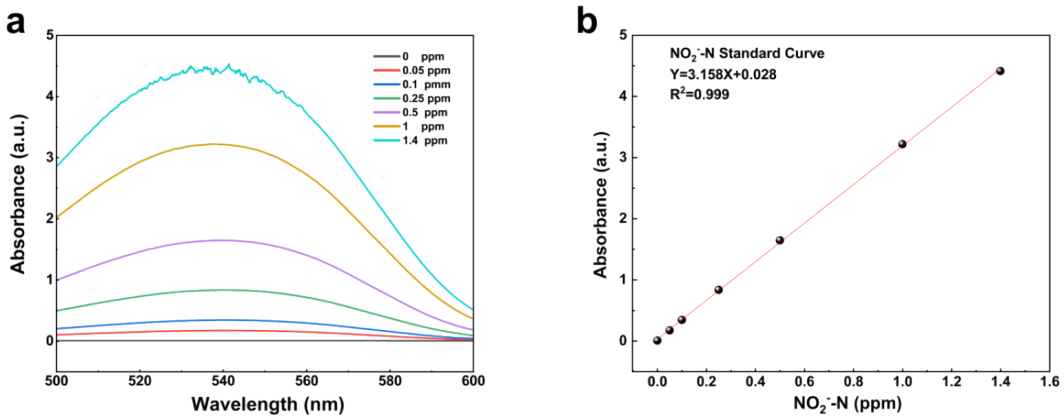


**Fig. S6** (a) UV-Vis absorption spectra of various $NO_2^-$-N concentrations (0, 0.05, 0.1, 0.25, 0.5, 1.0 and 1.4 ppm). (b) The calibration curve used for calculation of $NO_2^-$-N concentrations.

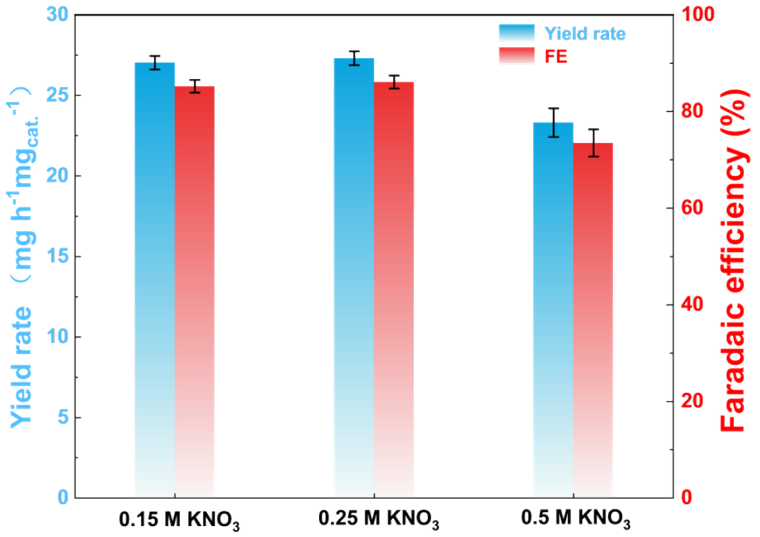


**Fig. S7** $NH_3$ Yield rate and FE in the electrolyte of KOH (0.1 M) and $KNO_3$ (0.15 M, 0.25 M and 0.5 M) at a current of 100 mA.

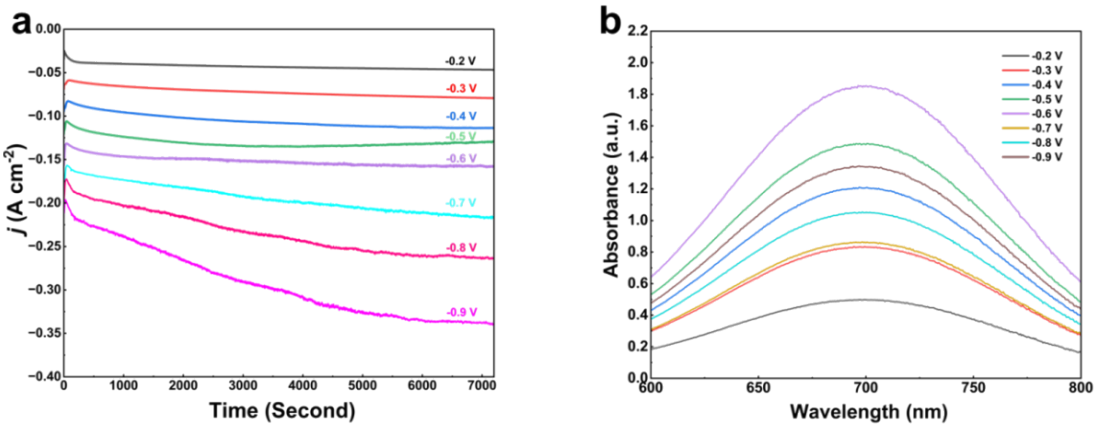


**Fig. S8** (a) The j-t curves at different potentials in 0.1 M KOH + 0.25 M $KNO_3$ electrolyte over a 2 h period. (b) UV-Vis absorption spectra of the corresponding samples.

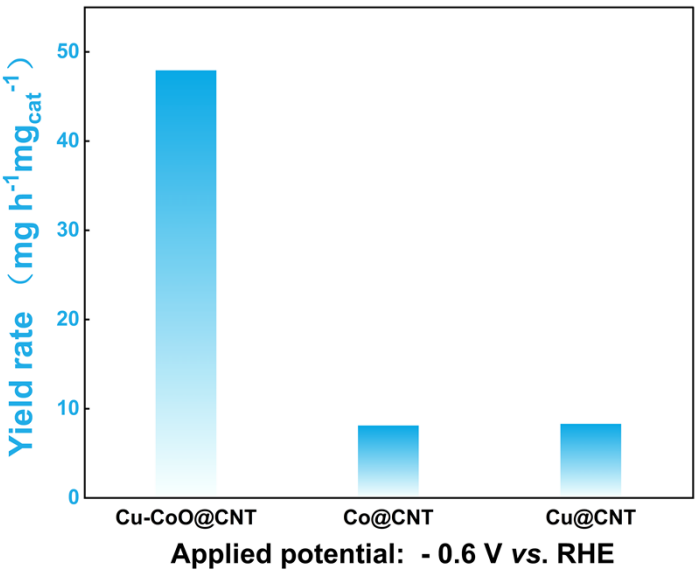


**Fig. S9** Comparison of $NH_3$ yield rate of Cu-CoO@CNT, Cu@CNT and Co@CNT.

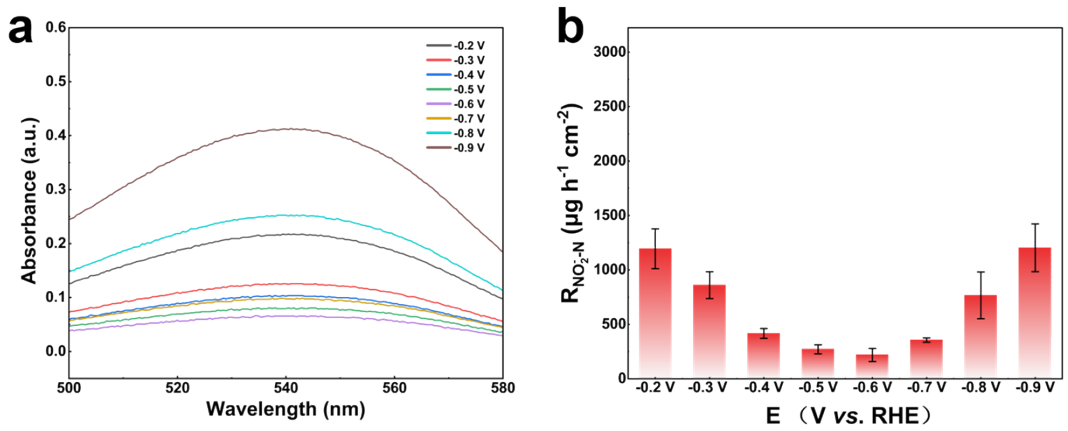


**Fig. S10** (a) UV-Vis absorption spectra of the corresponding samples. (b) The yield $NO_2^-$-N of $NO_2^-$ in different potentials between -0.2 to -0.9 V (vs. RHE).

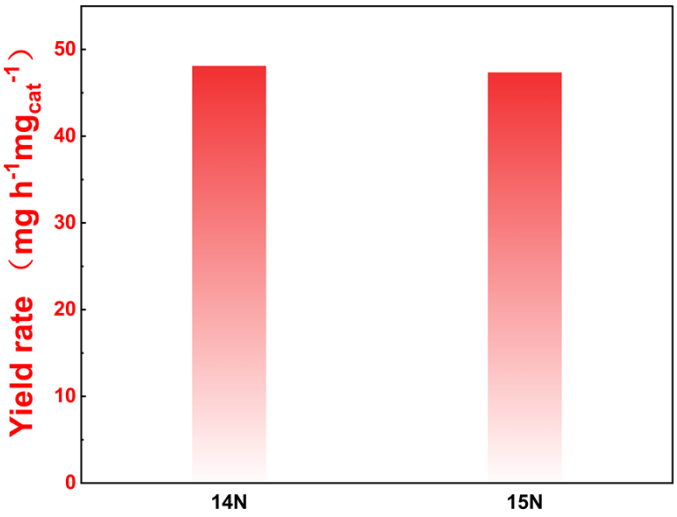


**Fig. S11** Comparison of $NH_3$ yield rate from Cu-CoO@CNT using $^{14}NO_3^-$ and $^{15}NO_3^-$ as nitrogen source, respectively.

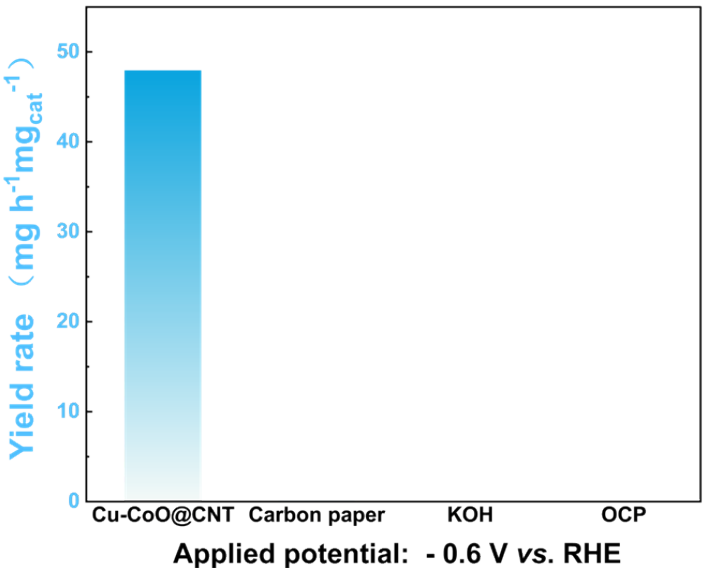


**Fig. S12** $NH_3$ yield rate contrast experiments with different conditions 0.1 M KOH, OCP, CP and Cu-CoO@CNT at −0.6 V (*vs*. RHE) for 2 h.

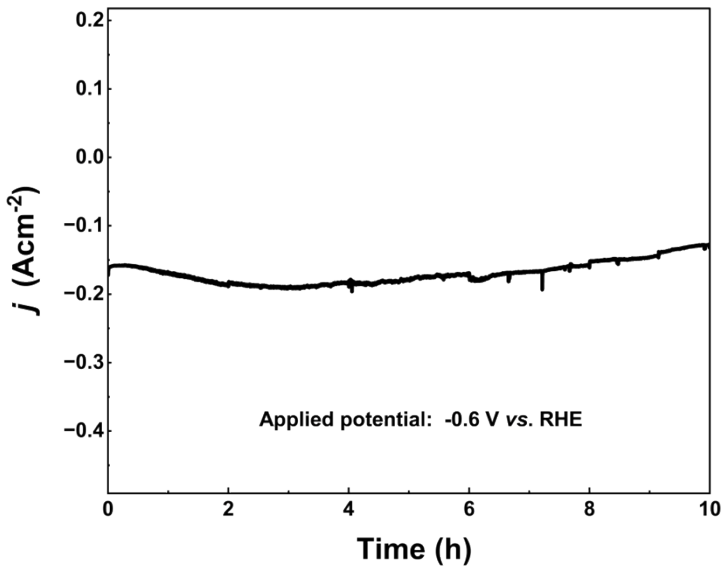


**Fig. S13** Long-time stability test of Cu-CoO@CNT at −0.6 V (*vs*. RHE).

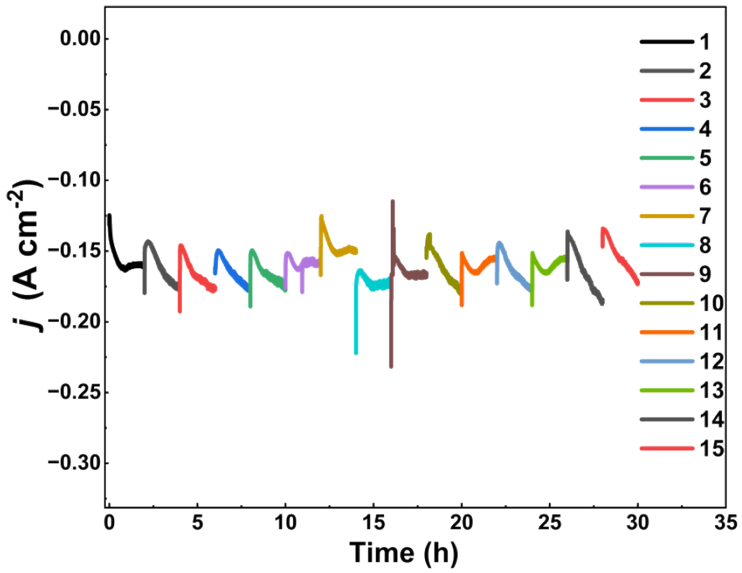


**Fig. S14** Cycling stability test of Cu-CoO@CNT at −0.6 V (*vs*. RHE) for 15 cycles with 2.0 h NtrRR period per cycle.

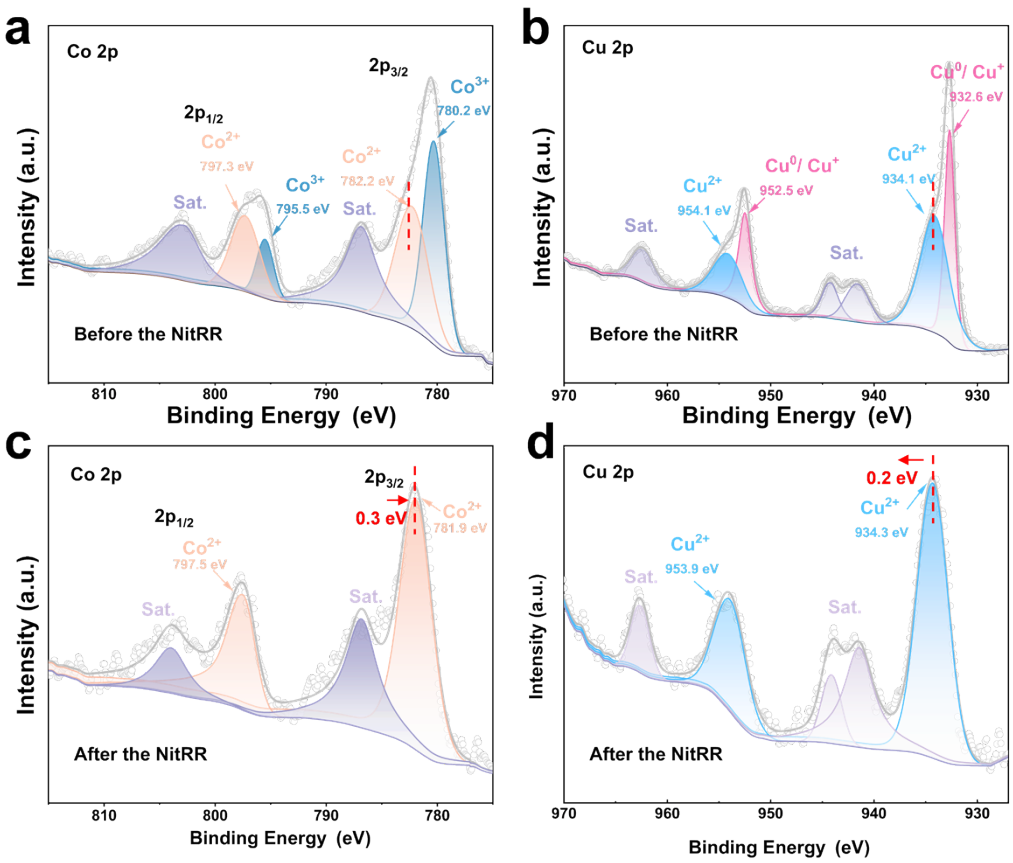


**Fig. S15** High-resolution XPS spectra of (a-b) Co 2p and (c-d) Cu 2p of Cu-CoO@CNT before and after NtrRR.

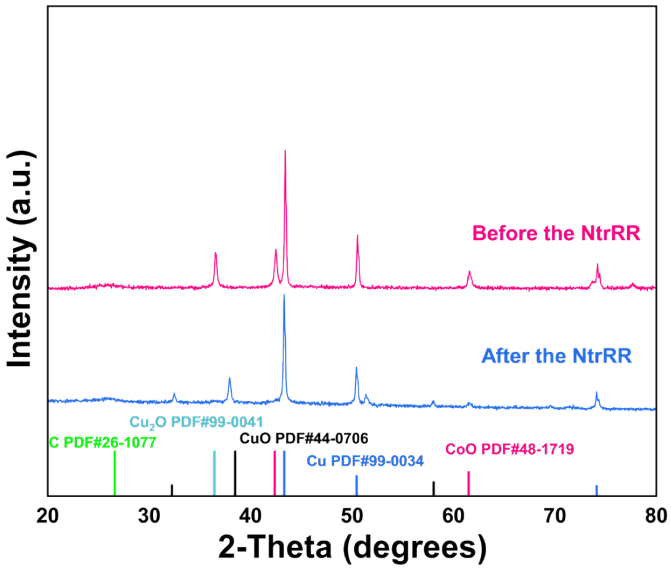


**Fig. S16** XRD patterns of Cu-CoO@CNT before and after NtrRR.

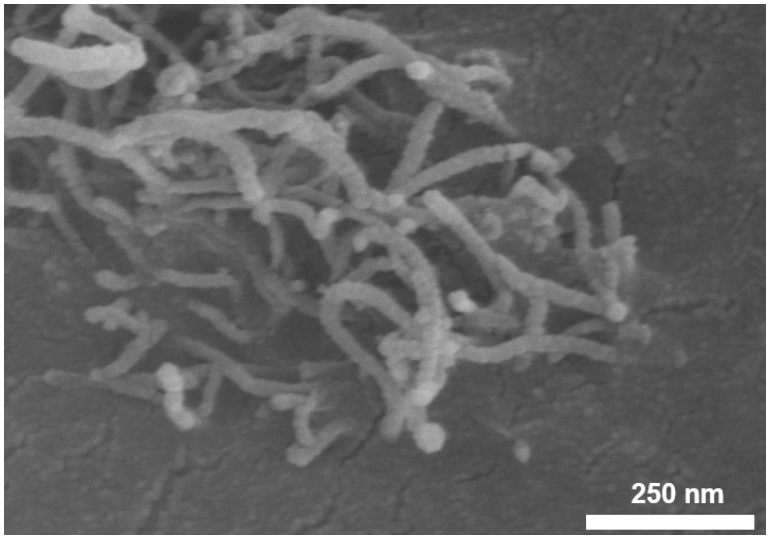


**Fig. S17** SEM image of Cu-CoO@CNT after 15 NtrRR recycles.

**Table S1. Surface content of different valence states of Cu and Co.**

| Class | Area (CPS.eV) | Content（%） |
|---|---|---|
| $Cu^{2+}$ | 37784.73 | 53.11 |
| $Cu^{0}/Cu^{+}$ | 33351.12 | 46.89 |
| $Co^{3+}$ | 18684.35 | 49.10 |
| $Co^{2+}$ | 19365.03 | 50.90 |

**Table S2. Comparison of NtrRR performance between Cu-CoO@CNT catalyst and others electrocatalysts recently-reported.**

| Catalyst | $NO_3^-$ concentration | Electrolyte | $NH_3$ yield rate ($mg\ h^{-1}mg_{cat.}^{-1}$) | FE(%) |
|---|---|---|---|---|
| NbC@CNFs[1] | 0.1 M | PBS | 16.7 | 81.7 (-1.1 V *vs*.RHE) |
| NiTP−CoTAPP[2] | 0.5 M | - | 2.723 | 85.6 (-0.8 V *vs*.RHE) |
| Ce-Cu/$MoO_2$@C[3] | 0.1 M | 1 M KOH | 20.3 | 92.0 (-0.4 V *vs*.RHE) |
| Cu/CoOOH[4] | 1400 ppm | 1 M KOH | 35.654 | 91.5 (-0.23 V *vs*.RHE) |
| RhNiAu-TML/Au-NC[5] | 50 mM | 0.1 M $HClO_4$ | 21.6 | 97.9 (+0.05 V *vs*.RHE) |
| Cu/$Fe_3O_4$@CN[6] | 0.1 M | 0.1 M KOH | 22.1 | 96.57 (-0.9 V *vs*.RHE) |
| BDCu[7] | 0.1 M | - | 25.74 | 96.58 (-1.8 V *vs*.SCE) |
| Fe-rGO[8] | 0.1 M | 0.1 M KOH | 47.815 | 96.51 (-0.5 V *vs*.RHE) |
| hcp/fcc $Cu_{10}Ni_{90}$[9] | 100 mM | 0.5 M $K_2SO_4$ | 57.4 | 98.1 (-0.7 V *vs*.RHE) |
| **This work** | 0.25 M | 0.1 M KOH | 83.2 | 98.1 (-0.6 V *vs*.RHE) |

## References


1 Z. Zhang, A. Niu, Y. Lv, H. Guo, J. S. Chen, Q. Liu, K. Dong, X. Sun and T. Li, *Angew. Chem. Int. Ed.*, 2024, **63**, e202406441.

2 Z. Zhang, M. Wang, H. Xing, X. Zhou, L. Gao, S. Chen, Y. Chen, H. Xu, W. Li, S. Yuan, C. Li, Z. Jin and J. Zuo, *Angew. Chem. Int. Ed.*, 2025, **64**, e202505580.

3 J. Dong, X. Song, Y. Chen, Z. Gai, Z. Yuan, D. Liu, Z. Tan, A. Liu, X. Wang and S. Song, *Adv Funct. Mater.*, 2025, **35**, 2422025.

4 X. Zhou, W. Xu, Y. Liang, H. Jiang, Z. Li, S. Wu, Z. Gao, Z. Cui and S. Zhu, *ACS Catal.*, 2024, **14**, 12251–12259.

5 W. Zhong, Q.-L. Hong, Q.-Y. Du, B. Y. Xia, X. Ai, F.-M. Li and Y. Chen, *Energy Environ. Sci.*, 2025, **18**, 4971–4981.

6 X. Cheng, H. Zhao, P. Liu, R. Han and Y.-Q. Wang, *J. Colloid Interface Sci.*, 2025, **682**, 703–714.

7 J. Wang, Z. Ou, C. Dong, M. Su, A. Ali, A. V. Kuklin, H. Ågren, G. V. Baryshnikov, Y. Liu, X. Zhao and H. Zhang, *ACS Catal.*, 2025, **15**, 156–166.

8 S. Li, J. Yan, M. Liu and H. Su, *J. Energy Chem.*, 2025, **103**, 682–691.

9 Y. Wang, F. Hao, H. Xu, M. Sun, X. Wang, Y. Xiong, J. Zhou, F. Liu, Y. Hu, Y. Ma, X. Meng, L. Guo, C. Wang, M. Shao, G. Wang, J. Wang, P. Lu, J. Yin, J. Wang, W. Niu, C. Ye, Q. Zhang, S. Xi, B. Huang, M. Shao and Z. Fan, *Angew. Chem. Int. Ed.*, 2025, **64**, e202508617.